Quantum Information and Computation, Vol. 17, No. 5&6 (2017) 0456–0468

ANALYTICAL EVIDENCE OF ULTRAFAST GENERATION OF SPIN-MOTION ENTANGLEMENT

KUO HAI[1,2], YUNRONG LUO[1,2], GUISHU CHONG[3], HAO CHEN[1], WENHUA HAI[1,2*]
[1] *Department of Physics and Key Laboratory of Low-dimensional Quantum Structures and Quantum Control of Ministry of Education, Hunan Normal University, Changsha 410081, China*
[2] *Synergetic Innovation Center for Quantum Effects and Applications, Hunan Normal University*
[3] *School of Physics and Microelectronics, Hunan University, Changsha 410082, China*

Received October 16, 2016
Revised April 3, 2017

We investigate ultrafast generation of spin-motion entanglement of a trapped and Gaussian-pulse-kicked two-level ion in the Lamb-Dicke limit and high field regime. A set of exact motional states and the probabilities occupying different pseudospin states are derived and the visible differences between the results with those of the delta-kick case are shown during a kick moment, which analytically evidence the ultrafast generation of an exact spin-motion entangled state regardless of initial state. Our results can be justified with the current experimental capability and provide an analytical method for further study of the ultrafast entanglement in atomic qubits.

Keywords: spin-motion entanglement; ultrafast generation; two-level ion; Gaussian-pulsed laser; delta kick
Communicated by: D Wineland & R Blatt

1. INTRODUCTION

The delta-kicked rotor and their variants have been investigated theoretically [1-15] and experimentally [16-28] as the paradigmatic systems of classical and quantum chaos. Many important phenomena, such as the quantum suppression of classically chaotic diffusion [16, 17], dynamical or pseudorandom Anderson localization [2, 14] and controlled decoherence [18, 19, 9] were found, which have been applied to study the quantum accelerator modes [20, 21], atom interferometer and precision measurements [10, 11, 12, 26], and the chaos-dependent quantum entanglements [24]. In the Lamb-Dicke regime when the particle moves in a range which is much smaller than the laser wavelength [25, 29, 30], the kicked-rotor model is reduced to that of a pulsed particle in a harmonic trap [31] or in an infinite square well [32]. Recently, the interesting ultrafast entanglement of a single atom's hyperfine spin state with its motional state has been demonstrated experimentally by using a short train of picosecond laser pulses [25, 26]. The ultrafast entanglement generation in superconducting circuits has also been studied by employing the dynamical Casimir effect [33-36]. The entanglement generation [37], entanglement breaking [38] and entanglement sudden death [39] were payed close attention in the areas of quantum information processing.

The coherent modification and control of entanglement were directly related to the basic quantum logic operations [40, 41]. Since the introduction of the optical tweezers [42], lasers

*Email address: whhai2005@aliyun.com

have been used extensively to push, trap and manipulate nano and microscopic particles. Particularly, applications of a train of short laser pulses which was approximated theoretically by a set of delta functions have led to rich physical phenomena [16, 17, 25, 26, 43]. However, as pointed out in Ref. [22], "so far, most of these studies have concentrated on the probability distribution rather than the full quantum state determined by amplitude and phase". The convoluted behaviors of the phases are at the heart of the phenomena of quantum interference and dynamical localization [22, 44].

For a quantum delta-kicked two-level particle, the detectable probabilities are related to the phases of the motional states [6, 22]. Because of the singularity of the first-order time-dependent Schrödinger equation, discontinuity of the solution arises and takes the form of jumping phase at the kick times [4, 22]. The jumping phase means that the unique state does not exist at the kick times. By using the Floquet time evolution operators, the quantum state just after (or before) a kick was given theoretically [6, 8, 14, 22, 25]. In terms of such discontinuous state, the probabilities $P_\alpha(T_+)$ or $P_\alpha(T_-)$ of finding the particle in the internal states $|g_\alpha\rangle$ ($\alpha = 1$ or 2) with T_+ (T_-) the time just after (before) a kick have been calculated numerically [6]. The phase jump at a kick moment $t = T$ may bring the difficulty of nonphysical probability hopping. Although such a probability-hopping difficulty rooted in the delta function has been overcome in experiments by applying a short train of laser pulses with finite width [25, 26, 43], *the corresponding analytical result involving the realistic Gaussian-pulse-kicked particle is scarce yet.* It is well-known that exact analytical solution can provide deeper understanding of the underlying physics in experiment than straight numerical calculations can [45].

In this paper, we consider a two-level cold ion confined in a harmonic trap and interacting with a short train of strong Gaussian-shaped laser pulses, and derive a set of exact solutions with continuously-varying phases in the Lamb-Dicke regime. The probability $P_\alpha(t)$ of the particle being in the internal pseudospin state $|g_\alpha\rangle$ is obtained as a function of time. At the kick moment $t = T$, it can change rapidly between $P_\alpha(T_+)$ and $P_\alpha(T_-)$ that leads to the ultrafast generation of an exact spin-motion entangled state (including the Schrödinger Kitten or bigger cat state defined in Ref. [46]) regardless of initial state. Comparing the results with those of the delta-kick case, visible differences of the evolution details are evidenced. The exact ultrafast transfer can be transparently manipulated by adjusting the pulse width and driving intensity in the existing experimental setup [25, 26, 43], and can be applied to further study the ultrafast entanglement in atomic qubits.

2. Exact monodromy and continuous probability

We investigate a single trapped particle with two stable internal ground states $|g_\alpha\rangle$ for $\alpha = 1, 2$, by applying a short train of ultrafast laser pulses. The experimentally relevant Gaussian-pulse kicks $f_g(t)$ can be approximated by a train of delta kicks $f_k(t)$ such that the Hamiltonian governing the system reads [6, 17, 25, 26]

$$H_{g,k}(x,t) = \frac{p^2}{2m} + V_0(x) + f_{g,k}(t)\sum_{\alpha=1}^{2} V_\alpha(x)|g_\alpha\rangle\langle g_\alpha|,$$

$$f_g(t) = \frac{1}{\sigma\sqrt{\pi}} \sum_{j=1}^{N} e^{-(t-jT)^2/\sigma^2}, \; f_k(t) = \sum_{j=1}^{N} \delta(t - jT) \tag{1}$$

with integer N labeling the number of pulses and parameter σ being the pulse width. In general, $V_0(x)$ is a trapped potential, $V_\alpha(x)$ may be a periodic function of x for a kicked rotor or is proportional to x for an electromagnet-pulsed particle held in an infinite square well [32]. The amplitude of $V_\alpha(x)$ denotes the interaction strength between the particle and the laser field, which is characterized by the Rabi frequency Ω_α that is much greater than the motional trap frequency in the strong excitation regime [25, 26]. The pulse width σ can be less than the order of picosecond for the ultrafast processes [25, 26]. Mathematically, the above approximation means $f_k(t) \approx \lim_{\sigma\to 0} f_g(t)$ with the nonphysical zero width of pulses. Periodically vanishing δ-function indicates that the Hamiltonian H_k is switched between two different operators periodically in time, leading to the nonphysical probability hopping. Physically, the width σ should be a nonzero constant related to the system parameter [6]. To overcome the probability-hopping difficulty and to fit an experiment, we can employ the well-behaved Gaussian pulses of finite width. The used method also can be extended to allow for other pulses, for example, a widely used sech-shaped Rosen-Zener pulse [47, 48].

We express the state vector as $|\Psi(x,t)\rangle = \frac{1}{\sqrt{2}} \sum_{\alpha=1}^{2} \psi_\alpha(x,t)|g_\alpha\rangle$, where $\psi_\alpha(x,t)$ is the external motional state entangling the corresponding internal pseudospin states $|g_\alpha\rangle$. Writing the motional state as $\psi_\alpha(x,t) = R_\alpha(x,t)e^{i\Theta_\alpha(x,t)}$ with amplitude $R_\alpha(x,t)$ and phase $\Theta_\alpha(x,t)$, the Schrödinger equation based on Eq. (1) is transformed to the real equations

$$\begin{aligned} \frac{\partial\Theta_\alpha}{\partial t} &= -\Big[\frac{1}{2m}\Big(\frac{\partial\Theta_\alpha}{\partial x}\Big)^2 + V_0 + V_\alpha f_\beta - \frac{\hbar^2}{2mR_\alpha}\frac{\partial^2 R_\alpha}{\partial x^2}\Big], \\ \frac{\partial R_\alpha}{\partial t} &= -\frac{1}{2m}\Big(R_\alpha\frac{\partial^2\Theta_\alpha}{\partial x^2} + 2\frac{\partial R_\alpha}{\partial x}\frac{\partial\Theta_\alpha}{\partial x}\Big) \end{aligned} \tag{2}$$

for $\beta = g$ or k. Direct integration to Eq. (2) over a kick gives

$$\begin{aligned} \Theta_\alpha(x, jT_+) - \Theta_\alpha(x, jT_-) &= \begin{cases} 0 & \text{for } \beta = g, \\ -V_\alpha(x) & \text{for } \beta = k, \end{cases} \\ R_\alpha(x, jT_+) - R_\alpha(x, jT_-) &= 0 \;\text{ for }\; j = 1, 2, ..., N, \end{aligned} \tag{3}$$

where $jT_\pm = jT \pm 0^+$ with 0^+ obeying $0 < 0^+ \ll 1$. This shows the continuity of $R_\alpha(x,t)$ and the discontinuity of $\Theta_\alpha(x,t)$ at $t = jT$ for $\beta = k$. The latter results in the relation [4, 22]

$$\psi_\alpha(x, jT_+) = \psi_\alpha(x, jT_-)e^{-iV_\alpha(x)} \tag{4}$$

and the jumping phase for $V_\alpha(x) \neq 0$, so that the state $\psi_\alpha(x, jT)$ cannot exist uniquely as $0^+ \to 0$. It is worth noting that the probability interpretation of quantum mechanics requires a monodromy probability, and the jumping phase at the kick times seem to be no problem for a single state. However, for a two-level particle the total quantum state is a linear superposition of the two basic vectors. After a $\pi/2$ pulse of Ramsey type experiment, the state is rotated to the form [6, 43]

$$|\Psi'(x,t)\rangle = \frac{1}{\sqrt{2}}[\psi_1'(x,t)|g_1\rangle + \psi_2'(x,t)|g_2\rangle] \tag{5}$$

with $\psi_1'(x,t) = \frac{1}{\sqrt{2}}(\psi_1 - \psi_2)$ and $\psi_2'(x,t) = \frac{1}{\sqrt{2}}(\psi_1 + \psi_2)$. For a harmonic potential $V_0(x)$, the motional states $\psi_\alpha'(x,t)$ with the exact solutions $\psi_\alpha(x,t)$ of Eq. (8) denote the generalized coherent states [49, 50] with spatially separated wave-packet positions. Consequently, the superposition state (5) can be an analogy to Schrödinger's cat state in Ref. [43], namely the spin-motion entangled state. However, at an initial or a final time, if the laser pulse does not act on the system, Eq. (5) may be a disentangled (or entangled) state with the linearly dependent (or independent) motional states $\psi_1(x,t)$ and $\psi_2(x,t)$. After an action of a ultrashort pulse, phase coherence between the two motional states $\psi_\alpha(x,t)$ makes the dependence of the measurable probability $P_\alpha(t)$ of the particle being in internal state $|g_\alpha\rangle$ on the phase $\Theta_\alpha(x,t)$. Noticing the normalization condition

$$\langle\Psi'(x,t)|\Psi'(x,t)\rangle = \langle\Psi(x,t)|\Psi(x,t)\rangle = \frac{1}{2}\sum_\alpha \langle\psi_\alpha(x,t)|\psi_\alpha(x,t)\rangle = 1,$$

from Eq. (5) we get [6]

$$\begin{aligned} P_1(t) &= \frac{1}{2}\{1 - Re[\langle\psi_2(x,t)|\psi_1(x,t)\rangle]\} \\ &= \frac{1}{2} - \frac{1}{2}\int_{-\infty}^{\infty} R_1 R_2 \cos(\Theta_1 - \Theta_2)dx, \end{aligned} \tag{6}$$

and $P_2(t) = 1 - P_1(t)$. Clearly, the time-dependent $P_\alpha(t)$ can describe the transitions between two internal states. At any time, the probability $P_\alpha(t) = 0$ for $\alpha = 1$ or 2 is associated with the disentangled states of Eq. (5). According to the form of the maximally entangled state of two spin-$\frac{1}{2}$ particles, we define the maximally spin-motion entangled state as Eq. (5) with $P_1(t) = P_2(t) = 1/2$ and for the linearly independent states $\psi_1(x,t)$ and $\psi_2(x,t)$. Therefore, after an action of a ultrashort pulse, the transition from a disentangled state to a maximally entangled state leads to the ultrafast generation of spin-motion entanglement.

Applying Eq. (3) to Eq. (6) yields $P_1(jT_+) - P_1(jT_-) \neq 0$ for $\beta = k$, and $P_1(jT_+) - P_1(jT_-) = 0$ for $\beta = g$. Consequently, the jumping phases for $\beta = k$ will bring the nonphysical probability hopping at $T_- \to T_+ \to T$. However, in the case $\beta = g$, Eq. (3) means that Eq. (6) is an exact monodromy and continuously-varying probability at $t = jT$. We will use it to evidence the ultrafast population transfer as follows.

3. Ultrafast generation of an exact spin-motion entangled state

Let us take a simplest example of Eq. (1) to analytically show that the nonphysical probability hopping exists for the system H_k and it can be suppressed by using the system H_g. The considered system is a two-level particle trapped in a harmonic potential $V_0(x)$ and driven by a pulsed laser standing wave. In the Lamb-Dicke regime and for a trapped ion in an appropriate position of the standing wave [29, 30], the system is governed by Eq. (1) with [6, 32, 31]

$$V_0(x) = \frac{1}{2}m\omega^2 x^2, \quad V_\alpha(x) = K_\alpha' \cos(kx - \phi) \approx K_\alpha x, \tag{7}$$

for $\alpha = 1, 2$ and $\phi = \pi/2$, and with m, ω, k being the particle mass, trap frequency and laser wave vector, respectively. The laser-atom (kick) interaction intensity $K_\alpha = kK_\alpha'$ is

proportional to the effective Rabi frequency Ω_α^2/Δ for a large detuning Δ between the laser frequency and the internal transition frequency [25]. The strong excitation regime means that the Rabi frequency is much greater than the motional trap frequency, so that we have the inequality [6, 25, 26] $|\Delta| \gg \Omega_\alpha \gg \omega$. Hereafter, time t and pulse period T in Eq. (1) are normalized in units of ω^{-1} which is evaluated in the interval of $10^{-8} \sim 10^{-5}$ second [29], spatial coordinate x is rescaled by the characteristic length $l = \sqrt{\frac{\hbar}{m\omega}}$ being in order of $0.1 \sim 100$nm, and the energy and driving intensity K_α are normalized by the harmonic oscillator level $\hbar\omega$ and energy density $\hbar\omega/l = \sqrt{m\hbar\omega^3}$, respectively. Experimental realization of the system (7) is well known for an atomic ion [25, 26] and for a neutral atom [16, 23]. Instead of the Lamb-Dicke approximation, one also can assume a pulse train much shorter than a trap period, such that trap evolution is negligible during the pulse sequence [26]. Alternately, for a charged particle the linear potential $K_\alpha x$ can be realized by an electromagnetic field [32]; while it can be produced by a magnetic field gradient applied along the x direction for a neutral atom [51, 52].

Exact solutions in the Lamb-Dicke regime. By applying the trial-solution method for solving the time-dependent Schrödinger equations [49, 50], we construct a set of exact solutions to Eqs. (2) and (7) as

$$\psi_\alpha(x,t) \to \psi_{\alpha n}(x,t) = R_{\alpha n}(x,t)e^{i\Theta_{\alpha n}(x,t)} \tag{8}$$

for $\alpha = 1, 2;\ n = 0, 1, 2, 3, ...$, where the real functions $R_{\alpha n}(x,t)$ and $\Theta_{\alpha n}(x,t)$ read

$$\begin{aligned} \Theta_{\alpha n}(x,t) &= -\Big(\frac{1}{2}+n\Big)\theta(t) + b_{\alpha 2}x + \frac{\dot\rho(t)}{2\rho(t)}x^2 + \gamma_\alpha(t), \\ R_{\alpha n}(x,t) &= \Big(\frac{\sqrt{c_0}}{\sqrt{\pi}2^n n!\rho(t)}\Big)^{\frac{1}{2}} H_n[\xi_\alpha(x,t)]e^{-\frac{1}{2}\xi_\alpha^2(x,t)}, \end{aligned} \tag{9}$$

with $H_n(\xi_\alpha)$ being the Hermite polynomial of the space-time combined variable

$$\xi_\alpha(x,t) = \frac{\sqrt{c_0}}{\rho(t)}x - \frac{b_{\alpha 1}(t)\rho(t)}{\sqrt{c_0}}. \tag{10}$$

In Eqs. (9) and (10), the real functions $\rho(t), \theta(t)$, $\gamma_\alpha(t), b_{\alpha 1}(t)$ and $b_{\alpha 2}(t)$ have the forms

$$\begin{aligned} &\rho(t) = \sqrt{\varphi_1^2 + \varphi_2^2}, \quad \theta(t) = \arctan\Big(\frac{\varphi_2}{\varphi_1}\Big), \\ &\gamma_\alpha(t) = \frac{1}{2}\int_0^t [b_{\alpha 1}^2(\tau) - b_{\alpha 2}^2(\tau)]d\tau + \gamma_\alpha(0), \end{aligned} \tag{11}$$

$$\begin{aligned} b_{\alpha 1}(t) &= \frac{K_\alpha}{\rho^2}\Big[\varphi_1\int_0^t f_\beta(\tau)\varphi_2(\tau)d\tau - \varphi_2\int_0^t f_\beta(\tau)\varphi_1(\tau)d\tau\Big] + b_{\alpha 1}(0), \\ b_{\alpha 2}(t) &= \frac{K_\alpha}{\rho^2}\Big[-\varphi_1\int_0^t f_\beta(\tau)\varphi_1(\tau)d\tau - \varphi_2\int_0^t f_\beta(\tau)\varphi_2(\tau)d\tau\Big] + b_{\alpha 2}(0) \end{aligned} \tag{12}$$

for $\beta = g$ or k. Here $\varphi_l = A_l\cos(t + B_l)$, $l = 1, 2$ are the real and imaginary parts of the solution to equation $\ddot\varphi = -\varphi$, A_i, B_i and $c_0 = \varphi_1\dot\varphi_2 - \varphi_2\dot\varphi_1 = A_1A_2\sin(B_1 - B_2)$ are the

constants to be determined by the form of the initial state. The auxiliary functions $\rho(t)$ and $\theta(t)$ are field-free, and functions $b_{\alpha 1}(t), b_{\alpha 2}(t)$ depend on the driving field $f_\beta(t)$. Applying $f_\beta(t)$ of Eq. (1) to the integrals in Eq. (12) gives the functions

$$\begin{aligned}
\int_0^t f_k(\tau)\varphi_l(\tau)d\tau &= \sum_{j=1}^{N}\int_0^t \delta(t-jT)\varphi_l(\tau)d\tau = \sum_{j=1}^{L} A_l\cos(jT+B_l),\\
\int_0^t f_g(\tau)\varphi_l(\tau)d\tau &= \frac{A_l}{\sigma\sqrt{\pi}}\sum_{j=1}^{N}\int_0^t \cos(\tau+B_l)e^{-(\tau-jT)^2/\sigma^2}d\tau\\
&= -\frac{A_l}{4}\sum_{j=1}^{N} e^{-\sigma^2/4}\Big\{e^{i(B_l+jT)}\Big[erf\Big(-\frac{jT}{\sigma}-\frac{i\sigma}{2}\Big)+erf\Big(\frac{jT-t}{\sigma}+\frac{i\sigma}{2}\Big)\Big]\\
&\quad +e^{-i(B_l+jT)}\Big[erf\Big(-\frac{jT}{\sigma}+\frac{i\sigma}{2}\Big)+erf\Big(\frac{jT-t}{\sigma}-\frac{i\sigma}{2}\Big)\Big]\Big\} \qquad (13)
\end{aligned}$$

for $l=1,2,\ L\le t<L+1,\ L=1,2,3,...$, where $erf(z)$ denotes the error function of z and σ is the pulse width. From Eq. (9) to Eq. (13) we clearly see that for the case $K_1\neq K_2$, Eq. (8) with $\alpha=1,2$ denotes two linearly independent states which result in the spin-motion entanglement in Eq. (5).

Noticing that in Eq. (9) $R_{\alpha n}(x,t)=R_{\alpha n}[\xi_\alpha(x,t),t]$ satisfies the harmonic oscillator equation $\frac{\rho^2}{c_0}\frac{\partial^2 R_{\alpha n}}{\partial x^2}=\frac{\partial^2 R_{\alpha n}}{\partial \xi_\alpha^2}=[\xi_\alpha^2-(2n+1)]R_{\alpha n}$, we can directly prove that Eq. (9) with Eqs. (10 - 13) is a set of exact solutions of Eq. (2). The exact solutions are $n+1$ complete solutions with some arbitrary constants and obey the orthonormalization condition $\langle\psi_{\alpha n}|\psi_{\alpha n'}\rangle=\delta_{n,n'}$. For a nonzero initial value $b_{\alpha 1}(0)$ in Eq. (10), Eqs. (9 - 13) mean that any state $\psi_{\alpha n}(x,t)$ with quantum number n is a generalized coherent state with $n+1$ wave packets [49, 50]. The ground state $\psi_{\alpha 0}(x,t)$ just is the well-known coherent state.

In order to determine the arbitrary constants in the exact solutions, we have to know the initial motional state $\psi_{\alpha n}(x,0)$ and the initial population $P_\alpha(0)$. For many applications in quantum information, the particle must be cooled and initialized to a nearly pure motional ground state [25]. Therefore, here we only consider a cold ion in the ground state with $n=0$. Assuming that one of the initial motional states obeys $\psi_{10}(x,0)=\psi_0(x)$ with $\psi_0(x)$ bing the harmonic oscillator ground state, Eqs. (9 - 12) imply the parameter equations

$$\begin{aligned}
&\frac{1}{2}\theta(0)=\frac{1}{2}\arctan\Big(\frac{A_2\cos B_2}{A_1\cos B_1}\Big)=\gamma_1(0),\\
&\dot\rho(0)=-\frac{A_1^2\sin(2B_1)+A_2^2\sin(2B_2)}{2\sqrt{A_1^2\cos^2 B_1+A_2^2\cos^2 B_2}}=0,\\
&\frac{\sqrt{c_0}}{\rho(0)}=\sqrt{\frac{A_1A_2\sin(B_1-B_2)}{A_1^2\cos^2 B_1+A_2^2\cos^2 B_2}}=1, \qquad (14)
\end{aligned}$$

and $b_{\alpha 1}(0)=b_{\alpha 2}(0)=0$.

Hopping and continuously-varying phases. Given the constants in Eq. (14) and the phase factor $b_{\alpha 2}(t)$ associated with the pulsed field f_β, from Eqs. (12) and (13) we can illustrate the phase jump for $f_\beta=f_k$ with pulse width $\sigma\to 0$ and the continuous phase for $f_\beta=f_g$ with finite pulse width. Let us take the parameter set $S=\{A_1=2,\ A_2=1,\ B_1=2.1863,\ B_2=$

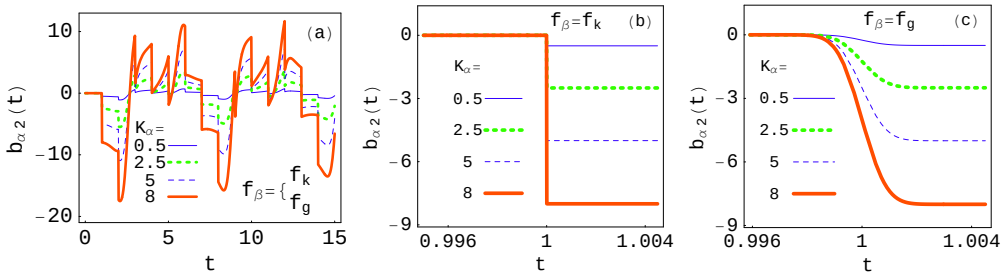

Fig. 1. Time evolutions of the field-related phase factors $b_{\alpha 2}(t)$ for the dimensionless parameter set $S = \{A_1 = 2,\ A_2 = 1,\ B_1 = 2.1863,\ B_2 = 0.6155,\ T = 1(\omega^{-1}),\ \sigma = 0.001(T)\}$ and the kick intensities $K_\alpha = 0.5$ (solid curves), $K_\alpha = 2.5$ (thick dashed curves), $K_\alpha = 5$ (dashed curves) and $K_\alpha = 8$ (thick solid curves). In (a), the short trains of $N = 15$ pulses are applied for both the delta-kicked field $f_\beta = f_k(t)$ and the Gaussian-pulsed field $f_\beta = f_g(t)$, resulting in two sets of curves which are coincident in the coarse-grained descriptions. The evolution details during the first kick time are shown, which reveal the phase jump in case (b) of delta kick and the continuously-varying phase in case (c) of Gaussian pulse. Here time t is in units of $\omega^{-1} = 10^{-7}$s and phase factors $b_{\alpha 2}(t)$ are dimensionless.

$B_1 - \frac{\pi}{2} = 0.6155,\ T = 1(\omega^{-1}),\ \sigma = 0.001(T)\}$ and a short train of $N = 15$ pulses as an example. Time evolutions of the field-related phase factors $b_{\alpha 2}(t)$ are plotted in Fig. 1 for four different values of kick intensity. Applying the driving fields $f_k(t)$ and $f_g(t)$, respectively, the plotted two sets of curves are shown in Fig. 1(a) by which we find that for any same K_α value the produced two curves are coarse-grained coincident, so the phase evolutions seem to be identical except for the evolution details during the kick time $t = j(T)$ exhibited in Fig. 1(b) and Fig. 1(c). This means that the delta-kick approximation works well in the coarse-grained dynamics, where the phase factors oscillate aperiodically with amplitudes being proportional to the kick intensities. The discernible differences are displayed in Fig. 1(b) with delta-kicked field and Fig. 1(c) with Gaussian-pulse-kicked field. In Fig. 1(b) we can see the phase jump at the first kick time with jump range positively related to the delta-kick intensity. The continuity of phase is shown in Fig. 1(c) for the Gaussian-shaped field $f_g(t)$, where at the first kick time the phase changes with different velocities which is positively related to the K_α value. For a greater K_α value the phase factor $b_{\alpha 2}(t)$ can change a large range during a quite short time. The quantum phase is associated to the expectation value of momentum [49, 50] $\overline{p} = \frac{1}{2}\sum_\alpha \langle \psi_{\alpha n}|\hat{p}|\psi_{\alpha n}\rangle$. Therefore, it is expectable that the fast change of momentum will cause the fast population transfer.

Broken and smooth wave-packet orbits. In the time evolution, center position of the particle's wave packets propagates along the trajectory $x_{\alpha c}(t)$ given by $\xi_\alpha(x_{\alpha c}, t) = 0$ in Eq. (10) with velocity $\dot{x}_{\alpha c}(t)$ in the forms [50]

$$x_{\alpha c}(t) = c_0^{-1}\rho^2(t)b_{\alpha 1}(t),\ \dot{x}_{\alpha c}(t) = c_0^{-1}\rho\dot{\rho}b_{\alpha 1} + b_{\alpha 2}. \tag{15}$$

Combining Eq. (15) with Eqs. (11), (12) and (13), we adopt the same parameters as those of Fig. 1 to plot time evolutions of the wave-packet centers for the driving fields $f_k(t)$ and $f_g(t)$, respectively. The produced two sets of curves are shown in Fig. 2(a), where the

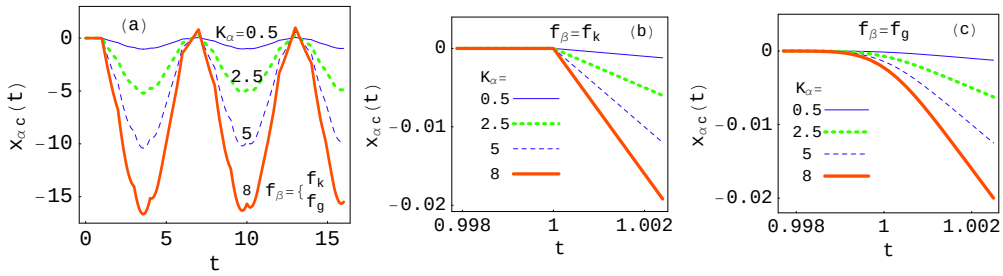

Fig. 2. Time evolutions of the wave-packet centers for the same parameters as those of Fig. 1, which display the approximately consistent periodic motions in (a) for both the delta-kick and Gaussian-pulse cases. The continuity of the wave-packet orbits and the broken trajectories are shown in (b) for $f_\beta = f_k$ at the first kick time. The wave-packet orbits are not only continuous but also smooth for $f_\beta = f_g$ at any time, as shown in (c). Here time t and positions $x_{\alpha c}(t)$ are in units of $\omega^{-1} = 10^{-7}$s and $\sqrt{\hbar/(m\omega)} = 1$nm, respectively.

coarse coincidence of the trajectories for the same K_α values and different driving fields is shown, which means approximate agreement between the two cases in the coarse-grained descriptions. The wave-packet centers oscillate near-periodically with period bing about $6(T)$ and amplitudes proportional to the kick intensities. The nonzero position difference $x_{1c}(t) \neq x_{2c}(t)$ for $K_1 \neq K_2$ means that the particle's wave function $|\Psi'(x,t)\rangle$ contains two spatially separated coherent harmonic oscillator ground states, that is the exact spin-motion entangled state, namely a Schrödinger Kitten state which is defined as a quantum superposition of coherent states with small amplitudes [46]. If one of the kick intensities K_1 and K_2 is increased and the trapped frequency ω is decreased sufficiently to make the position difference $|x_{1c}(t) - x_{2c}(t)|$ a bigger distance, the exact entangled state becomes a Schrödinger bigger cat state defined in Ref. [46], which was prepared experimentally by application of a sequence of laser pulses [43]. In Figs. 2(b) and 2(c), we observe that every trajectory is continuous at the kick time $t = 1$ for both cases, while only the trajectories of Fig. 2(c) with $f_\beta = f_g$ smoothly evolve. A cusp corresponding to the kick time exists for the delta-kick case that implies the nonphysical velocity hopping of the wave-packet motions. This agrees with Fig. 1 in which the jumping phase factors $b_{\alpha 2}$ is just a part of the velocity $\dot{x}_{\alpha c}(t)$ in Eq. (15).

Ultrafast generation of an exact spin-motion entangled state. We are interested in the ultrafast population transfer from any initial state to an exact spin-motion entangled state. This can be demonstrated by time evolutions of the probability. Combining Eq. (6) with Eqs. (8), (9) and (10), for $n = 0$ we easily arrive at

$$\begin{aligned} P_1(t) &= \frac{1}{2} - \frac{\sqrt{c_0}}{2\sqrt{\pi}\rho}\int_{-\infty}^{\infty} e^{-\frac{1}{2}(\xi_1^2+\xi_2^2)}\cos(\Theta_{10}-\Theta_{20})dx \\ &= \frac{1}{2} - \frac{\sqrt{c_0}}{2\sqrt{\pi}\rho}\int_{-\infty}^{\infty} e^{-\frac{c_0}{\rho^2}(x-\mu)^2+\nu^2}\cos[(b_{12}-b_{22})x+\gamma]dx \\ &= \frac{1}{2} - \frac{1}{2}\cos[(b_{12}-b_{22})\mu+\gamma]e^{\nu^2-\frac{\rho^2}{4c_0}(b_{12}-b_{22})^2}, \end{aligned} \tag{16}$$

where

$$\mu = \frac{\rho^2}{2c_0}(b_{11}+b_{21}), \quad \nu = \frac{\rho}{2\sqrt{c_0}}(b_{11}-b_{21}),$$
$$\gamma = \gamma_1 - \gamma_2 = \frac{1}{2}\int_0^t [b_{11}^2(\tau) - b_{12}^2(\tau) - b_{21}^2(\tau) + b_{22}^2(\tau)]d\tau + \gamma(0)$$

with $\gamma(0) = \gamma_1(0) - \gamma_2(0)$. Noticing $b_{\alpha 1}(0) = b_{\alpha 2}(0) = 0$ and Eq. (16), it is clear that the initial phase $\gamma(0)$ is determined by the initial population $P_1(0) = \frac{1}{2} - \frac{1}{2}\cos[\gamma(0)] = \sin^2[\gamma(0)/2]$. The typical initial values $P_1(0) = 0, \frac{1}{2}, 1$ correspond to the initial phases $\gamma(0) = 0, \frac{\pi}{2}, \pi$, respectively. After fixing the values of $A_{1,2}$, the constants $B_{1,2}, \gamma_1(0)$ and c_0 are given by Eq. (14), then the second initial motional states $\psi_{20}(x,0)$ is fixed by $\gamma(0)$ for the considered initial state $\psi_{10}(x,0) = \psi_0(x)$. In Eq. (16) we can see that the time evolution of the probability $P_1(t)$ depends on a product of the cosine function and exponential function. We define the exponential function associated with the driving field $f_\beta(t)$ as the transfer function

$$\begin{aligned} F_\beta(t) &= \exp\left[\nu^2 - \frac{\rho^2}{4c_0}(b_{12}-b_{22})^2\right] \\ &= \exp\left[\frac{\rho^2}{4c_0}\Big((b_{11}-b_{21})^2 - (b_{12}-b_{22})^2\Big)\right]. \end{aligned} \tag{17}$$

Applying Eq. (12) to Eq. (17), we know that the quantities in the square brackets are proportional to $(K_1 - K_2)^2$. When the laser intensity is set to obey $K_1 - K_2 = 0$, the transfer function is equal to 1 and Eq. (16) gives the constant probabilities $P_1 = \sin^2[\gamma(0)/2]$ and $P_2 = \cos^2[\gamma(0)/2]$ for any driving, which are related to the initial phase $\gamma(0)$. For two different kicked intensities with difference $K = |K_1 - K_2| \neq 0$, the transfer function may tend to zero with the increase of time, leading to the population transfer. Thus, Eq. (16) means that starting with any initial probability $P_1(0)$, the final population is certainly $P_1(t_f) = P_2(t_f) = \frac{1}{2}$ for the final time t_f. Such a population corresponds to the maximally entangled state of Eq. (5) with two linear independent motional states. To fix the final population, we should switch off the laser pulses just after the final time. Such a final population implies that the particle is transferred from any initial state to an exact spin-motion entangled state with different wave-packet positions [29, 43], $x_{1c}(t > t_f) \neq x_{2c}(t > t_f)$, as shown in Fig. 2. We define the transfer time $\Delta t_f = t_f - t_1$ by the equations $F_\beta(t_f) \approx 0$ and $F_\beta(t_1) \approx 1$, which is just the time required to reach the fully entangled state. When the initial probabilities $P_1(0) = 0$ and 1 are selected, the particle occupies a single internal state initially. Then application of the ultrashort pulses results in the ultrafast entanglement of the internal state with the motional state for a very short transfer time, namely the entanglement generation time [26]. For the initial probability $P_1(0) \neq 0, 1$, the initial state is an entangled state such that the ultrafast population transfer occurs between two entangled states. Overall, the arbitrariness of initial state enable us to recover spin-motion entanglement of the cold particle at any time.

The above assertions are verified by Fig. 3 for the parameter set S of Fig. 1 and four different difference values $K = 2, 4, 6, 8$ of the kick intensities. Time evolutions of the transfer functions are plotted in Fig. 3(a) for $N = 2$ pulses and both the $f_\beta = f_k(t)$ and $f_\beta = f_g(t)$ with pulse width $\sigma = 10^{-3}$. Two coarsely identical sets of curves are produced, where fast decays of the transfer functions at the first kick time and their part revivals and decays at

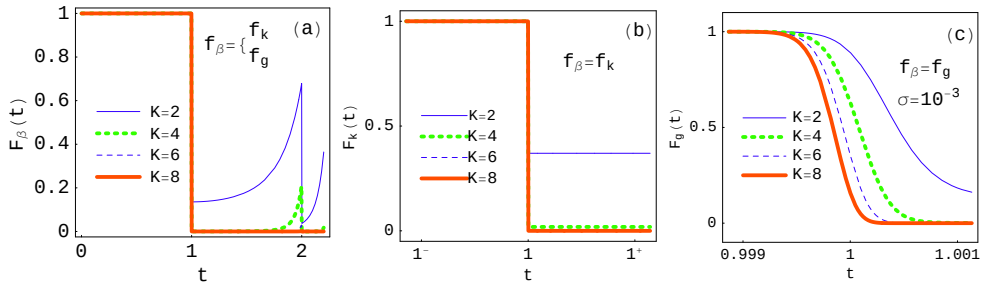

Fig. 3. Time evolutions of the transfer functions $F_\beta(t)$ for the parameter set S of Fig. 1 and the differences of kick intensities $K = 2$ (solid curves), $K = 4$ (thick dashed curves), $K = 6$ (dashed curves) and $K = 8$ (thick solid curves). The short trains of $N = 2$ pulses are applied for both the $f_\beta = f_k(t)$ and $f_\beta = f_g(t)$ with pulse width $\sigma = 10^{-3}$ respectively, and the coarse coincidence between the two sets of curves are shown in (a). The evolution details during the first kick time are displayed in (b) for $f_\beta = f_k(t)$ and $K \geq 4$ with hopping time obeying $\Delta t_f < 1^+ - 1^- \approx 10^{-16}$, and in (c) for $f_\beta = f_g(t)$ and $K \geq 4$ with transfer time $\Delta t_f \approx 0.001$. Here time t is in units of 10^{-7}s and functions $F_\beta(t)$ are dimensionless.

the second kick time are shown, which mean the corresponding transfers of the occupance probability of the initial states. In Figs. 3(b) and 3(c), details of the time evolutions of the transfer functions $F_k(t)$ and $F_g(t)$ are plotted during the first kick time. In Fig. 3(b), the transfer function $F_k(t)$ jumps from 1 to 0 during the time interval $\Delta t_f < 1^+ - 1^- \approx 10^{-16}(T)$ and for the strong laser-atom interactions with a larger difference $K = |K_1 - K_2| \geq 4$, indicating the nonphysical probability hopping. The transfer function $F_g(t)$ changes rapidly from 1 to 0 during the transfer time $\Delta t_f \approx 0.001(T)$ in Fig. 3(c) for $K \geq 4$, which exhibits the fast population transfer.

The delta-kicked field is a limit of the Gaussian-pulsed field with the pulse width σ tending zero. In Fig. 3(c) we find that a finite σ value corresponds to a finite transfer time t_f, and Fig. 3(b) implies that $\sigma \to 0$ leads to the nonphysical result $\Delta t_f \to 0$. Therefore we desire a ultrashort transfer time by applying a ultrafast pulse with very small width σ. This assertion is illustrated in Fig. 4 for the same parameters and driving field as those of Fig. 3(c) except for (a) $\sigma = 10^{-4}$ and (b) $\sigma = 10^{-5}$. Selecting the time unit as $\omega^{-1} = T = 10^{-7}$s, the pulse width $\sigma = 10^{-4}$ corresponds to the transfer time $\Delta t_f \sim 1.0001 - 0.9999 = 2 \times 10^{-4}(T) = 10^{-11}$s, as shown in Fig. 4(a). By decreasing the σ value to picosecond $10^{-5}(T) = 10^{-12}$s, we plot Fig. 4(b) which indicates the corresponding transfer time as $\Delta t_f \sim 1.00001 - 0.99999 = 2 \times 10^{-5}(T) = 2 \times 10^{-12}$s, displaying the occurrence of a fast population transfer [26]. By further decreasing the pulse width to femtosecond scale, we can realize the exact ultrafast population transfers in several femtoseconds theoretically. However, the limits of the applicability exist, when the pulse widths become comparable to an optical cycle, which happens at the fs scale. To model pulses of such short lengths, the oscillatory dynamics and phases of the electric field at the optical frequency should become important. In the ultrafast processes, the probability associated with any K value is evaluated uniquely. From the analysis on Eqs. (16) and (17) and the observations to Figs. 3 and 4, we find the parameter regions in which the maximally entangled state with $P_1 = P_2 = \frac{1}{2}$ can be reached by seeking the parameter condition vanishing

the transfer functions after a transfer time.

According to Eq. (14), we have also selected different initial constants $A_{1,2}, B_{1,2}$ and $\gamma_{1,2}(0)$ to illustrate the transfer functions $F_\beta(t)$ and some similar results are obtained, which are not shown here.

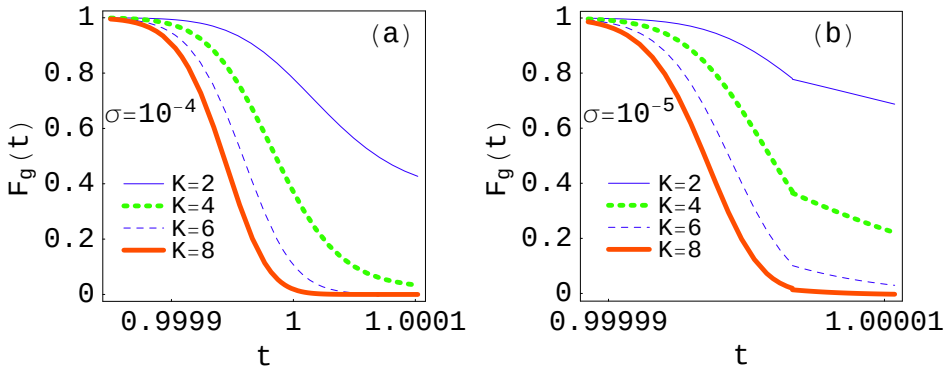

Fig. 4. Time evolutions of the transfer functions for the same parameters and driving field as those of Fig. 3(c) except for the pulse widths (a) $\sigma = 10^{-4}$ and (b) $\sigma = 10^{-5}$ which corresponds to a picosecond pulse. The fast population transfers with transfer time of picosecond order are shown in (b). Here the used units are the same as those of Fig. 3.

4. Conclusion and discussion

We have investigated a cold two-level particle confined in a harmonic trap by applying a short train of strong Gaussian-shaped laser pulses. Under the Lamb-Dicke limit, the nonphysical probability-hopping difficulty of a quantum kicked system is revealed and an analytical method for overcoming the difficulty is established, through a set of exact solutions of the considered system with continuously-varying phases. The exact probability $P_\alpha(t)$ of the particle occupying internal pseudospin state $|g_\alpha\rangle$ is obtained. In the high field regime, the probability change continuously and rapidly during any kick moment, which results in ultrafast generation of an exact spin-motion entangled state, including the well-known Schrödinger Kitten and bigger cat states [46]. The similar Schrödinger cat state has been prepared experimentally by applying a sequence of laser pulses [43]. Our results provide an analytically quantitative method to transparently control and speed up the generation process of the accurate spin-motion entanglement by decreasing the pulse width and increasing the driving intensity.

The exact ultrafast population transfers include the ultrafast entanglement of internal state with motional state and the transfer between two entangled states, and can be observed in the current experimental setup [25, 26, 43]. However, there exist some sources of dissipation and damping in these experiments [29], which were believed to be in part due to the uncontrolled magnetic-field fluctuations at the ion position, the frequency and intensity fluctuations of the applied light fields, and the unexpectedly high heating rate out of the motional ground state. The corresponding decoherence of a superposition state [29] is commonly interpreted as a

way of quantifying the elusive boundary between classical and quantum worlds and almost always precludes the existence of entangled states, except at extremely short time scales [43]. Applications of the considered ultrashort pulses and coherent states (classical-like wave packets) allow a suppression of decoherence in the experiments of controlling atomic qubits [25, 26], and may provide insight into the boundary between the classical and quantum worlds [43].

The used method and obtained results can be extended to allow different pulses produced by more advanced pulses shaping techniques [25, 26], such as the widely used Rosen-Zener pulses [47, 48] and other local pulses. In fact, using any train of pulses instead of $f_g(t)$ in Eq. (1), exact solutions in the similar forms as Eqs. (9 - 13) exist such that the similar ultrafast processes can be observed under a different external field. Thus a potential application could be to purposefully design time-optimal pulse trains with varying amplitude and phase to get coherent control of the particle from an initial quantum state to a desired final state.

Although the exact solutions in Eq. (9) are related to different forms of pulses for different α, Figs. 1(a), 2(a) and 3(a) show that all of the coarse-grained dynamics look identical regardless of whether delta kicks or Gaussian pulses are used. The visible differences between the both cases are clearly exhibited in the panels (b) and (c) of Figs. 1, 2 and 3. Because the delta-kicked rotor and their variants are the most studied paradigmatic systems of classical and quantum chaos, it is also important for us to analytically evidence the differences. Our results prompt that the delta-kick is analytically applicable as proxies for very short pulses if one only cares about the coarse-grained dynamics, for example, in the field of classically chaotic dynamics where the interesting dynamics surely show up in the coarse-grained description of the system. However, if a unpredictable quantum event occurs during a microscopic time interval which is related to the kick moment, we have to apply the realistic pulse with finite width to resolve the phase jump problem.

Acknowledgements

This work was supported by the NNSF of China under Grant Nos. 11475060 and 11204077, the Construct Program of the National Key Discipline of China.

References

1. Casati G, Chirikov B V, Izraelev F M, and Ford J 1979 Lecture Notes in Physics (Springer, Berlin), **93** 334
2. Fishman S, D. Grempel D R, and Prange R E 1982 Phys. Rev. Lett. **49** 509
3. Blümel R, Meir R and Smilanski U 1984 Phys. Lett. A **103** 353
4. Grempel D R, Prange R E, and Fishman S 1984 Phys. Rev. A **29** 1639
5. Lima R and Shepelyansky D 1991 Phys. Rev. Lett. **67** 1377
6. Gardiner S A, Cirac J I, and Zoller P 1997 Phys. Rev. Lett. **79** 4790
7. Xie Q and Hai W 2005 Eur. Phys. J. D **33** 265
8. McDowall P, Hilliard A, McGovern M, Grünzweig T, and Andersen M F 2009 New J. Phys. **11** 123021
9. Romanelli A 2009 Phys. Rev. A **80** 022102
10. Tonyushkin A, Wu S, and Prentiss M 2009 Phys. Rev. A **79** 051402 (R)
11. Horne R A, Leonard R H, and Sackett C A 2011 Phys. Rev. A **83** 063613
12. Daszuta B and Andersen M F 2012 Phys. Rev. A **86** 043604

13. Hernández G and Romanelli Al 2013 Phys. Rev. A **87** 042316
14. Ermann L and Shepelyansky D L 2014 J. Phys. A **47** 335101
15. Floss J and Averbukh I S 2015 Phys. Rev. E **91** 052911
16. Moore F L, Robinson J C, Bharucha C F, Williams P E, and Raizen M G 1994 Phys. Rev. Lett. **73** 2974
17. Moore F L, Robinson J C, Bharucha C F, Sundaram B and Raizen M G 1995 Phys. Rev. Lett. **75** 4598
18. Klappauf B G, Oskay W H, Steck D A and Raizen M G 1998 Phys. Rev. Lett. **81** 1203
19. Szriftgiser P, Ringot J, Delande D, and Garreau J C 2002 Phys. Rev. Lett. **89** 224101
20. d'Arcy M B, Godun R M, Oberthaler M K, Cassettar D and Summy G S 2001 Phys. Rev. Lett. **87** 074102
21. Wimberger S, Guarneri I and Fishman S 2004 Phys. Rev. Lett. **92** 084102
22. Bienert M, Haug F, Schleich W P and Raizen M G 2002 Phys. Rev. Lett. **89** 050403
23. Jones P H, Stocklin M M, Hur G and Monteiro T S 2004 Phys. Rev. Lett. **93** 223002
24. Chaudhury S, Smith A, Anderson B E, Ghose S and Jessen P S 2009 Nature **461** 768
25. Hayes D, Matsukevich D N, Maunz P, Hucul D, Quraishi Q, Olmschenk S, Campbell W, Mizrahi J, Senko C and Monroe C 2010 Phys. Rev. Lett. **104** 140501
26. Mizrahi J, Senko C, Neyenhuis B, Johnson K G, Campbell W C, Conover C W S and C. Monroe 2013 Phys. Rev. Lett. **110** 203001
27. Gadway B, Reeves J, Krinner L and Schneble D 2013 Phys. Rev. Lett. **110** 190401
28. Lopez M, Clément J-F, Lemarié G, Delande D, Szriftgiser P and Garreau J C 2013 New J. Phys. **15** 065013
29. Leibfried D, Blatt R, Monroe C and Wineland D J 2003 Rev. Mod. Phys. **75** 281
30. Wu Y and Yang X X 1997 Phys. Rev. Lett. 78 3086
31. Chen H, Tan J, Hai K, Zhang X, Hai W 2015 Eur. Phys. J. D **69** 278
32. Hogg T and Huberman B A 1982 Phys. Rev. Lett. **48** 711
33. S. Felicetti, M. Sanz, L. Lamata, G. Romero, G. Johansson, P. Delsing, and E. Solano, 2014 Phys. Rev. Lett. **113**, 093602
34. D. Z. Rossatto, S. Felicetti, H. Eneriz, E. Rico, M. Sanz, and E. Solano, 2016 Phys. Rev. B **93**, 094514
35. C. M. Wilson, G. Johansson, A. Pourkabirian, M. Simoen, J. R. Johansson, T. Duty, F. Nori and P. Delsing, 2011 Nature **479**, 376
36. B. Schneider, M. Simoen, I. M. Svensson, A. Bengtsson, T. Aref, J. Bylander, Progress in Electromagnetic Research Symposium. Shanghai, 2314 (2016).
37. Rafiee M and Bayat A 2014 Quantum Inf. Comput. **14** 0777
38. King C 2014 Quantum Inf. Comput. **14** 1203
39. Yonac M and Eberly J H 2014 Quantum Inf. Comput. **14** 0039
40. Solenov D 2016 Quantum Inf. Comput. **16** 0954
41. Ma T, Jing J, Guo Y, and Yu T 2016 Quantum Inf. Comput. **16** 0597
42. Askin A 1970 Phys. Rev. Lett. **24** 156
43. Monroe C, Meekhof D M, King B E, Wineland D J 1996 Science **272** 1131
44. Hai K, Luo Y, Lu G and Hai W 2014 Opt. Express **22** 4277
45. Zakrzewski J 1985 Phys. Rev. A **32** 3748
46. Ourjoumtsev A, Tualle-Brouri R, Laurat J, Grangier P 2006 Science **312**, 83
47. Gould P L, Ruff G A, and Pritchard D E 1986 Phys. Rev. Lett. **56** 827
48. Vitanov N V and Knight P L 1995 Phys. Rev. A **52** 2245
49. Hai W, Xie Q, and Fang J 2005 Phys. Rev. A **72** 012116
50. Lu G, Hai W and Xie Q 2006 J. Phys. A **39** 401
51. Chen Y A, Nascimbène S, Aidelsburger M, Atala M, Trotzky S and Bloch I 2011 Phys. Rev. Lett. **107** 210405
52. Ma R, Tai M E, Preiss P M, Bakr W S, Simon J and Greiner M 2011 Phys. Rev. Lett. **107** 095301